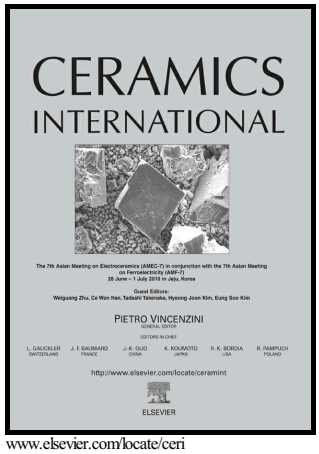

www.elsevier.com/locate/ceri

Microwave assisted hydrothermal synthesis of $(Fe,Co)_3O_4$ nanoparticles in the presence of surfactants and effects of Co/Fe ratio on microstructure and magnetism

Miloš Ognjanović, Biljana Dojčinović, Martin Fabián, Dalibor M. Stanković, José F.M.L. Mariano, Bratislav Antić

PII: S0272-8842(18)31119-2
DOI: https://doi.org/10.1016/j.ceramint.2018.04.246
Reference: CERI18163

To appear in: *Ceramics International*

Received date: 28 February 2018
Revised date: 24 April 2018
Accepted date: 28 April 2018

Cite this article as: Miloš Ognjanović, Biljana Dojčinović, Martin Fabián, Dalibor M. Stanković, José F.M.L. Mariano and Bratislav Antić, Microwave assisted hydrothermal synthesis of $(Fe,Co)_3O_4$ nanoparticles in the presence of surfactants and effects of Co/Fe ratio on microstructure and magnetism, *Ceramics International,* https://doi.org/10.1016/j.ceramint.2018.04.246

Microwave assisted hydrothermal synthesis of $(Fe,Co)_3O_4$ nanoparticles in the presence of surfactants and effects of Co/Fe ratio on microstructure and magnetism

Miloš Ognjanović[1*], Biljana Dojčinović[2], Martin Fabián[1,3], Dalibor M. Stanković[1,4], José F. M. L. Mariano[1,5] and Bratislav Antić[1]

[1]The "Vinča" Institute of Nuclear Sciences, University of Belgrade, POB 522, 11001 Belgrade, Serbia

[2]Institute of Chemistry, Technology and Metallurgy, University of Belgrade, Studentski trg 12-16, 11000 Belgrade

[3]Institute of Geotechnics, Slovak Academy of Sciences, Watsonova 45, 04001, Košice, Slovakia

[4]Innovation Center of the Faculty of Chemistry, University of Belgrade, POB 522, 11001 Belgrade, Serbia

[5]Department of Physics and CeFEMA, Faculty of Science and Technology, University of Algarve, Campus de Gambelas, Faro 8005-139, Portugal

*corresponding author: Miloš Ognjanović, The "Vinča" Institute of Nuclear Sciences, University of Belgrade, P. O. Box 522, 11000 Belgrade, Serbia. E-mail: miloso@vin.bg.ac.rs Phone: 00381 11 3336829

Abstract

Microstructure and magnetic properties of nanoparticles can be tailored by optimising the synthesis procedure and changing chemical composition. In this study, a two-step procedure, i.e., coprecipitation in the presence of PEG 300 followed by microwave assisted (MW) hydrothermal synthesis, was introduced to obtain $Co_xFe_{3-x}O_4$ (x = 0, 0.1 and 0.2) nanoparticles. It was found that with the increase of Co content, particle/crystallite size increased, with significant change of coercivity (H_c). The mixed samples of $Co_xFe_{3-x}O_4$ (x = 0.1 and 0.2) were magnetically harder in comparison with Fe_3O_4. The H_c of Fe_3O_4 was 91 Oe, while for $Co_{0.10}Fe_{2.90}O_4$ and $Co_{0.20}Fe_{2.80}O_4$, H_c was 256 Oe and 1070 Oe, respectively. Saturation magnetisation (M_s) of mixed samples also increased up to 6% compared to Fe_3O_4. A special effort was devoted to study the effects of introducing different surfactants (PEG 300, PEG 4000 or SDS) during the synthesis procedure in order to improve morphological and microstructural properties of $CoFe_2O_4$ nanoparticles. The influence of surfactants on physical/chemical properties of nanoparticles is discussed.

Keywords: Magnetite; microwave synthesis; cobalt ferrite; structural characterisation; magnetic properties.

1. Introduction

Nanoscale spinel ferrites MFe_2O_4 (metal M = Co, Mg, Mn, Zn, etc.) have been subjects of very intense research because of their potential applications in several technological fields including permanent magnets [1], magnetic fluids [2], magnetic hyperthermia [3], drug delivery [4] and high density information storage [5].

The crystal structure of spinel ferrites can be described as a cubic closed-packed arrangement of oxygen atoms with Me^{2+} and Fe^{3+} at two different crystallographic sites.

These sites have tetrahedral (A-sites) and octahedral (B-sites) oxygen coordination, and thus, the resulting local symmetries of both sites are different. If the A-sites are completely occupied by Fe^{3+} cations and the B-sites are randomly occupied by Me^{2+} and Fe^{3+} cations, the structure is referred to as an inverse spinel. Actually, real systems crystallise in a partially inverse structure with the following general formula [6]: $(M_{\delta}^{II}Fe_{1-\delta}^{III})[M_{1-\delta}^{II}Fe_{1+\delta}^{III}]O_4$.

Among the various magnetic materials, cobalt ferrite ($CoFe_2O_4$) has been widely studied because it possesses excellent chemical and thermal stabilities [7], good mechanical properties [8], strong magnetic anisotropy, moderate magnetisation, and high coercivity at room temperature [9]. $CoFe_2O_4$ shows a predominantly inverse structure with Co^{2+} ions mainly on octahedral sites (square bracket) and Fe^{3+} ions almost equally located between octahedral and tetrahedral sites (round bracket), but the observed inversion degree is often lower than 1 [10].

Different chemical synthesis methods, such as precipitation [11], sol-gel [12], hydrothermal [13], microemulsions [14], and solution combustion [15] are used to produce ferrite nanoparticles. On top of that, microwave assisted (MW) hydrothermal synthesis has been recognised as a very efficient method. Homogenous heating without thermal gradient effects leads to nanoparticles with relatively narrow size distribution [16]. In comparison with classical hydrothermal synthesis, MW hydrothermal synthesis offers great advantages as a simple, fast and very energy efficient procedure [17]. We applied a MW hydrothermal method as a second step after co-precipitation in order to obtain monodisperse $CoFe_2O_4$ and cobalt substituted magnetite ($Co_xFe_{3-x}O_4$).

For many applications, it is crucial to chemically stabilise magnetic nanoparticles (MNPs) against agglomeration in the course of synthesis or after synthesis. Suitable strategies include coating MNPs with organic species, including surfactants or polymers, or coating MNPs with an inorganic layer, such as carbon or silica [18]. It is noteworthy that protecting shells not only stabilises nanoparticles, but can also be used for modification of size/shape and further functionalisation of particles.

In this paper, we report a modified synthesis route to obtain nanocrystalline $Co_xFe_{3-x}O_4$ (x = 0, 0.1, 0.2 and 1) using a co-precipitation method at room temperature followed by MW hydrothermal synthesis at 200 °C. The prepared nanoparticles were characterised by X-ray powder diffraction (XRPD), Fourier transform-infrared spectroscopy (FT-IR), transmission electron microscopy (TEM), zeta potential measurements and dynamic light scattering (DLS) techniques. The magnetic properties were investigated using a SQUID magnetometer. Special effort was devoted to studying the effects of various surfactants applied during the synthesis process on the structural and morphological properties of $CoFe_2O_4$.

2. Experimental

2.1. Chemicals

Iron(II) sulphate heptahydrate ($FeSO_4 \cdot 7H_2O$, ACS reagent, ≥99.0%), cobalt(II) chloride ($CoCl_2$, purum p.a., anhydrous, ≥98.0%), ammonium hydroxide solution (NH_4OH, ACS reagent, 28,0-30,0% NH_3 basis), sodium oleate (≥82% oleic acid basis), citric acid (ACS reagent, ≥99.5%) and polyethylene glycol 1000 (PEG 1000, for synthesis) were purchased from Sigma Aldrich. Iron(III) chloride hexahydrate ($FeCl_3 \cdot 6H_2O$, ACS reagent, ≥99.0%),

polyethylene glycol 300 (PEG 300, for synthesis), polyethylene glycol 4000 (PEG 4000, for synthesis) and sodium dodecyl sulphate (SDS, $C_{12}H_{25}OSO_2ONa$, Ph Eur grade, ≥85.0 %) were purchased from Merck, Germany.

2.2. Synthesis of magnetite nanoparticles

The nanoparticles were synthesised using a co-precipitation method at room temperature followed by hydrothermal treatment in a microwave field at 200 °C.

i) Synthesis of $Co_xFe_{3-x}O_4$ (x = 0, 0.1, 0.2 and 1) magnetic nanoparticles.

Demineralised water (320 ml) was degassed during 30 min in an ultrasonic bath and kept for 15 min under a stream of N_2 in a 500 ml three-neck round bottom flask. After, the system was stored for 15 min at room temperature with vigorous mechanical stirring and under a blanket of nitrogen. Corresponding amounts of salts, iron(III) chloride hexahydrate, iron(II) sulphate heptahydrate, cobalt(II) chloride, and PEG 300 were weighed: mol Fe(III)/(mol (Fe(II) + Co(II)) = 0.030 / 0.015. Salts and PEG 300 (10 g/l in reaction mixture) were added to degassed water. After complete dissolution of the salts, 22.5 ml of ammonium hydroxide was slowly introduced dropwise for 60 min at constant stirring until pH 10 was reached in order to precipitate nanoparticles from the supernatant. The overall volume of the mixture was divided into seven vessels each with a volume of 100 ml. Each vessel contained 50 ml of mixture. The vessels were placed in a HPR-1000/10S high pressure segmented rotor and heated in the microwave digester ETHOS 1, Advanced Microwave Digestion System, MILESTONE, Italy. The power of microwave irradiation was set in the range of 0-1000 W, with linear heating of the mixture at 20 °C/min. The mixture was then heated at 200 °C for 20 min at maximum pressure of 100 bars. Following

completion of this hydrothermal synthesis assisted by microwave radiation, vessels were rapidly cooled in an air flow. The obtained nanoparticles were separated from the supernatant with the help of an external permanent magnet. The precipitate was then washed through several cycles with demineralised water until showing negative reactions to chlorides and sulphates, and finally, the nanoparticles were dispersed in water. The synthesised nanoparticles were dried for 24 h at 60 °C. After drying, the residue was triturated in an agate mortar. Nanoparticles with different metal compositions were obtained according to stoichiometry of the starting powders. Their chemical composition was studied by means of inductively coupled plasma-optic emission spectrometry (ICP-OES) performed on a Thermo Scientific iCAP 6500 Duo ICP system (Thermo Fisher Scientific, Cambridge, United Kingdom) spectrometer with iTEVA operational software. The samples were labelled on the basis of their actual composition as $Co_xFe_{3-x}O_4$ _PEG 300 (x = 0, 0.1, 0.2 and 1).

To improve the colloid stability of the prepared MNPs, their surface was further modified by another shell of surfactant. For this purpose, three different surfactants, citric acid (CA) (0.6 mmol/g), oleic acid (OA) (2 mmol/g), or PEG 1000 (5 mmol/g) were used for post-coating processes (optimal amounts were taken from E. Tombácz *et al.*[19]). The surfactant coated nanoparticles were labelled as CA@MNP_PEG 300, OA@MNP_PEG 300 and PEG 1000@MNP_PEG 300, respectively.

ii) Surfactant assisted synthesis of $CoFe_2O_4$ nanoparticles

In order to examine the effect of surfactants on the synthesis, three different surface-active agents were used: PEG 300 (10 g/l), PEG 4000 (10 g/l) and SDS (1 g/l). The stabilisers

were added to the reaction mixture before the addition of ammonium hydroxide. The obtained nanoparticles were labelled according to surfactant as $CoFe_2O_4$_PEG 300, $CoFe_2O_4$_PEG 4000 and $CoFe_2O_4$_SDS, respectively. For comparison, $CoFe_2O_4$ was also prepared without addition of any surfactant in the reaction procedure.

2.3. Experimental techniques

X-ray powder-diffraction (XRPD) patterns of synthesised nanoparticles were collected by use of a Rigaku SmartLab® X-ray diffractometer equipped with a Cu Kα source (λ = 1.54056 Å). The data were collected in the 2θ range from 10^o to 80^o with a step of 0.05° and exposition time of 3 s per step. The XRPD patterns were examined by SmartLab Studio and PDXL software programmes. The mean crystallite size, $<D_{XRPD}>$, was obtained by Scherrer's equation [20] ($< D_{XRPD} >= \frac{K \cdot \lambda}{\beta \cdot \cos\theta}$) where, K is constant related both to the crystallite shape and to the definition on both β and $<D_{XRPD}>$, λ is the wavelength of the X-rays, and β is the full-width at half maximum of the particular diffraction peak. K is assumed to equal 0.9. The $<D_{XRPD}>$ values were determined from (220), (311), (400), (422), (511) and (400) reflections.

The morphology, particle size and size distribution of the prepared MNPs were analysed by transmission electron microscopy (TEM) using a JEOL JEM 2100 operating at 200 kV. The mean particle size, $<D_{TEM}>$, was obtained by measuring the average diameter of 400-500 particles using images collected in different parts of the grid. To estimate the polydispersity of the sample with respect to the average particle size, an empirical parameter was defined as polydispersity index, σ_{TEM} (%), and it was evaluated as the ratio between the standard deviation and the average particle size [21]. The images were

analysed by Image J [22] software in manual mode. The nanoparticle size distributions were fitted using the log-normal function: $y = y_0 + \frac{A}{\sqrt{2\pi}\omega x} \exp \frac{-\left[\ln\frac{x}{x_c}\right]^2}{2\omega^2}$.

FT-IR spectra were recorded in the region from 400 cm^{-1} to 4000 cm^{-1} (with resolution of 0.5 cm^{-1}) using a Nicolet iS50 FT-IR, Thermo Fisher Scientific spectrophotometer equipped with a Smart iTR attenuated total reflectance (ATR) sampling accessory, by placing powder samples on the diamond plate and fixing them with a pressure tower.

Zeta potentials of the surfaces of modified MNPs (CA@MNP_PEG 300, OA@MNP_PEG 300 and PEG 1000@MNP_PEG 300) were measured on water colloidal dispersions at 25.0 ± 0.1 ^{o}C using a Nano NZ (Malvern) apparatus with a 4 mW He-Ne laser source (λ = 633 nm). The electrophoretic mobilities of MNPs were determined at pH ~ 6.5.

The average particle size of CA, OA and PEG 1000 covered nanoparticles were determined at 25.0 ± 0.1 ^{o}C on an instrument employing photon cross correlation spectroscopy, PCCS (NANOPHOX, Symphatec, Germany) equipped with a He-Ne laser (λ = 632.8 nm, max 10 mW).

Magnetic properties were studied by means of a Quantum Design MPMS XL SQUID (H_{max} = 70 kOe) and Quantum Design VersaLab VSM (H_{max} = 30 kOe). Magnetisation vs. magnetic field curves were measured at 300 K between -30 kOe and 30 kOe. Magnetisation vs. temperature was measured between 5 K and 300 K.

3. Results and discussion

3.1. Composition and microstructure of $Fe_{3-x}Co_xO_4$

The chemical composition of the prepared MNPs was checked by ICP-OES technique. The Fe/Co ratios were in accordance with stoichiometric ratios of the starting compounds. The

crystal structure of the prepared nanoparticles was investigated by XRD. The diffraction patterns of $Co_xFe_{3-x}O_4$ prepared using the PEG 300 surfactant assisted procedure are shown in Figure 1a. All reflections can be indexed in the cubic spinel structure type. The increase of Co^{2+} content in samples resulted in a shift of highly intense (311) reflection to lower 2θ angles, as shown in Figure 1b. The mean crystallite size of the studied samples, determined from Scherrer's equation, are listed in Table 1, and show similar values for Fe_3O_4 and cobalt substituted Fe_3O_4, but a significantly lower value for $CoFe_2O_4$.

TEM micrographs and particle size distributions (Figure 1c and 1d) indicate that the nanoparticles had high crystallinity. From their corresponding size distribution diagrams, it can be seen that the smallest particles (8.2 ± 2.0 nm) were observed for pure cobalt ferrite, denoting that the concentration of cobalt strongly influenced the particle size. When the concentration of cobalt precursor is high enough, the nucleation becomes spontaneous, while low concentration of precursor slows down the nucleation and allows growth of nanoparticles.

The fingerprint region of FT-IR spectra showed Me–O (Me = Co, Fe) stretching modes of spinel ferrites (Figure 1e). From this figure, it can be clearly seen that the metal-oxygen stretching mode of the octahedral and tetrahedral sites moved towards higher values with the increase of cobalt content, i.e. from 550 cm^{-1} for Fe_3O_4 to 567 cm^{-1} for $CoFe_2O_4$. Taking into account the values reported in the literature for pure magnetite (570 cm^{-1}) and cobalt ferrite (575 cm^{-1}) [23], this trend can be interpreted as gradual substitution of iron ions by cobalt ones within the spinel structure.

The zeta potentials of the post-surface functionalised MNPs were lower than -30 mV (see Figure S1), indicating stable dispersions. The MNP suspensions were agglomerated with a

mean hydrodynamic diameter (D_h) varying between 200 nm ($CoFe_2O_4$) and 330 nm ($Co_{0.2}Fe_{2.8}O_4$).

<<<Preferred position for Table 1>>>

<<<Preferred position for Figure 1>>>

3.2. Magnetic properties of $Co_xFe_{3-x}O_4$

Hysteresis loops with finite coercive fields and temperature dependent magnetisation were recorded for the studied MNPs (Figure 2a and 2b). All M(H) curves show hysteresis behaviour without any anomalous shape. The values of saturation magnetisation (M_s), coercivity (H_c) and remnant magnetisation (M_r) are summarised in Table 2. All values, H_c, M_r and M_s, reached maximum for $Co_{0.2}Fe_{2.8}O_4$.

The increase of magnetic parameters can be attributed to enhancement of the anisotropy due to selective occupation of Co^{2+} ions at cation sites in the Fe_3O_4 phase. Maintaining a high M_s is important in order to minimise the amount of material required to achieve the desired magnetic response for different applications, in particular those focused on medical therapies, which can be achieved by partial substitution of Fe^{2+} by Co^{2+}. The influence of cobalt concentration in $Co_xFe_{3-x}O_4$ was reported by Byrne et al. [24]. However, their obtained absolute values of magnetic parameters [24] were significantly smaller in comparison to our synthesised $Co_{0.2}Fe_{2.8}O_4$.

Reduced remnant magnetisation (M_r/M_s) was 0.35 for $Co_{0.1}Fe_{2.9}O_4$ and 0.41 for $Co_{0.2}Fe_{2.8}O_4$, respectively. Although the value of 0.41 is far from the expected for pure cubic anisotropy results (the theoretical value is 0.83 [25]), this suggests that gradual substitution of Co^{2+} leads to mixed cubic/uniaxial anisotropic nanoparticles, whereas Fe_3O_4

and $CoFe_2O_4$ nanoparticles possess uniaxial anisotropy. These data indicate that by inserting Co^{2+} ions and consequently, decreasing the Fe^{2+} concentration, both an increase of the saturation magnetisation and an increase of the anisotropy are produced compared with non-substituted nanoparticles. However, for pure $CoFe_2O_4$, decrease of saturation magnetisation and decrease of the anisotropy was noticed. This trend of M_s decrease and approximation to superparamagnetic state (lower H_c compared to $Co_{0.1}Fe_{2.9}O_4$ and $Co_{0.2}Fe_{2.8}O_4$) can be attributed to the reduction of $CoFe_2O_4$ particle size to 8.2 ± 2.0 nm, which resulted in higher surface-to-volume ratio and bigger disorder on the nanoparticle surface compared to other nanoparticles (surface effects) [26].

Information about the blocking temperature (T_B) of the nanoparticles was obtained through examination of the field-cooled (FC) and zero-field-cooled (ZFC) magnetisation collected at 100 Oe. The T_B is defined as the point above which the sample exhibits superparamagnetism such that the nanoparticle magnetisation is free to align in random orientations. The data show that T_B is above room temperature with no discernible peak visible below 300 K (Figure 2b).

<<<Preferred position for Figure 2>>>

<<<Preferred position for Table 2>>>

3.3. Composition, microstructure and morphology of $CoFe_2O_4$ prepared in surfactant free and surfactant assisted synthesis

The XRPD patterns of four samples of $CoFe_2O_4$, with the actual Co content equal in all of the samples ($x \sim 0.98$ in $Co_xFe_{3-x}O_4$, according to results of inductively coupled plasma optic emission spectroscopy, ICP-OES) are presented in Figure 3a. The nanoparticles were prepared without any or with addition of one of three different surfactants (PEG 300, PEG 4000 or SDS) during the synthesis procedure (see Experimental section). All XRPD reflections matched well with the unique cubic spinel structure ($CoFe_2O_4$, PDF card #221086). Lattice parameter and mean crystallite size are summarised in Table 3. The sharp and strong peaks reveal high crystallinity of the synthesised nanoparticles. Calculated values of lattice parameters were in the range of 8.36-8.38 Å, which are in good agreement with a reported value of ≈ 8.37 Å for cobalt ferrite [27]. It was found that the average crystallite size reduced with addition of surfactants, from 7.9 nm for $CoFe_2O_4$ to 5.8 nm for $CoFe_2O_4$_SDS. For $CoFe_2O_4$_PEG 300 and $CoFe_2O_4$_PEG 4000, calculated mean crystallite sizes were 6.6 and 6.4 nm, respectively.

Fourier transform-infrared spectroscopy (FT-IR) analysis was carried out in order to study the capping agent and to estimate organic phase content (Figure 3b). Two of the samples ($CoFe_2O_4$_SDS and $CoFe_2O_4$_PEG 4000) showed absorption bands at 3337 cm^{-1} and 1643 cm^{-1}, suggesting the presence of O–H stretching vibrations and symmetric H–O–H bending. Absorption bands at 1480 cm^{-1} and 1350 cm^{-1} indicated that the particles were capped by –CH_2 and =SO_2 groups [28]. The sample $CoFe_2O_4$_SDS also showed vibration typical for =SO group at 1053 cm^{-1}, which can be attributed to excess of surfactant in solution.

To further characterise the particle size and morphology of the nanoparticles, TEM analysis was performed, and results are presented in Figure 3c. TEM micrographs showed pseudo-spherical log-normally distributed nanoparticles with a mean diameter of 12.2 nm and a polydispersity index of 25% for $CoFe_2O_4$. Samples $CoFe_2O_4$_PEG 300 and $CoFe_2O_4$_PEG 4000 had reduced particle diameters of 8.2 nm (Figure 3d), while the sample coated with SDS had a diameter of 8.4 nm.

In the current study, we found that surfactants played a fundamental role in reducing crystallite/particle size. It is worth mentioning that an increase of particle size and change of shape when PEG is used as surfactant has been reported [29]. In the case of SDS, it was observed that particle size increases or decreases according to SDS concentration [30].

<<<Preferred position for Table 3>>>

<<<Preferred position for Figure 3>>>

4. Conclusions

The $Co_xFe_{3-x}O_4$ spinel structured samples were synthesised using a novel synthesis approach which was a combination of coprecipitation and MW assisted hydrothermal synthesis. The subsequent effects of cobalt concentration on particle size evolution and magnetic properties were demonstrated. The magnetisation measurements showed the highest coercivity (1070 Oe) and saturation magnetisation (77.8 emu g^{-1}) for $Co_{0.2}Fe_{2.8}O_4$ nanoparticles. The presence of surfactants significantly influenced the size of synthesised $CoFe_2O_4$ nanoparticles. This method of synthesis offers the possibility to change the

microstructure and magnetic properties of nanoparticles by tailoring chemical composition and preparation procedure.

Acknowledgment

This work was supported by the Ministry of Education, Science and Technological Development of the Republic of Serbia through the Eureka Project, E!9982.

Conflicts of interest

The authors declare that they have no conflict of interest.

References

[1] Y. Kitamoto, S. Kantake, F. Shirasaki, M. Abe, M. Naoe, Co ferrite films with excellent perpendicular magnetic anisotropy and high coercivity deposited at low temperature, J. Appl. Phys. 85 (8) (1999) 4708–4710.

[2] M.-P. Pileni, Magnetic Fluids: Fabrication, Magnetic Properties, and Organization of Nanocrystals, Adv. Funct. Mater. 11 (5) (2001) 323–336.

[3] D.H. Kim, S.H. Lee, K.H. Im, K.N. Kim, K.M. Kim, I.B. Shim, M.H. Lee, Y.-K. Lee, Surface-modified magnetite nanoparticles for hyperthermia: Preparation, characterization, and cytotoxicity studies, Curr. Appl. Phys. 6 (2006) e242-e246.

[4] W.S. Prestvik, A. Berge, P.C. Mork, P.M. Stenstad, J. Ugelstad, U. Hafeli, W. Schutt, J. Teller, M. Zborowski, Scientific and Clinical Applications of Magnetic Carriers, Plenum Press, New York (1997).

[5] A. Goldman, Modern Ferrite Technology, Van Nostrand Reinhold, New York, 1990.

[6] G. Blasse, New type of superexchange in the spinel structure some magnetic properties of oxides $Me^{2+}Co_2O_4$ and $Me^{2+}Rh_2O_4$ with spinel structure, Philips Res. Rep. 18 (1963) 383-392.

[7] J. Haetge, C. Suchomski, T. Brezesinski, Ordered mesoporous MFe_2O_4 (M= Co, Cu, Mg, Ni, Zn) thin films with nanocrystalline walls, uniform 16 nm diameter pores and high thermal stability: Template-directed synthesis and characterization of redox active trevorite, Inorg. Chem. 49 (24) (2010) 11619–11626.

[8] D. López, I. Cendoya, F. Torres, J. Tejada, C. Mijangos, Preparation and characterization of poly(vinyl alcohol)-based magnetic nanocomposites. 1. Thermal and mechanical properties, J. Appl. Polym. Sci. 82 (13) (2001) 3215–3222.

[9] B.D. Cullity, C.D. Graham, Introduction to magnetic materials, 2nd ed., Wiley, Hoboken, N.J., Chichester, 2009.

[10] G.A. Petitt, D.W. Forester, Mössbauer Study of Cobalt-Zinc Ferrites, Phys. Rev. B 4 (11) (1971) 3912–3923.

[11] V. Blaskov, V. Petkov, V. Rusanov, L. Martinez, B. Martinez, J.S. Muñoz, M. Mikhov, Magnetic properties of nanophase $CoFe_2O_4$ particles, J. Magn. Magn. Mater. 162 (2-3) (1996) 331–337.

[12] J.-G. Lee, J.Y. Park, C.S. Kim, Growth of ultra-fine cobalt ferrite particles by a sol–gel method and their magnetic properties, J. Mater. Sci. 33 (15) (1998) 3965–3968.

[13] S. Moosavi, S. Zakaria, C.H. Chia, S. Gan, N.A. Azahari, H. Kaco, Hydrothermal synthesis, magnetic properties and characterization of $CoFe_2O_4$ nanocrystals, Ceram. Int. 43 (10) (2017) 7889–7894.

[14] V. Pillai, D.O. Shah, Synthesis of high-coercivity cobalt ferrite particles using water-in-oil microemulsions, J. Magn. Magn. Mater. 163 (1-2) (1996) 243–248.

[15] B. Pourgolmohammad, S.M. Masoudpanah, M.R. Aboutalebi, Synthesis of $CoFe_2O_4$ powders with high surface area by solution combustion method: Effect of fuel content and cobalt precursor, Ceram. Int. 43 (4) (2017) 3797–3803.

[16] S. Yoon, Facile microwave synthesis of $CoFe_2O_4$ spheres and their application as an anode for lithium-ion batteries, J. Appl. Electrochem. 44 (9) (2014) 1069–1074.

[17] S. Komarneni, Nanophase materials by hydrothermal, microwave-hydrothermal and microwave-solvothermal methods, Curr. Sci. (2003) 1730–1734.

[18] S. Laurent, D. Forge, M. Port, A. Roch, C. Robic, L. Vander Elst, R.N. Muller, Magnetic iron oxide nanoparticles: synthesis, stabilization, vectorization, physicochemical characterizations, and biological applications, Chem. Rev. 108 (6) (2008) 2064–2110.

[19] E. Tombácz, I.Y. Tóth, D. Nesztor, E. Illés, A. Hajdú, M. Szekeres, L. Vékás, Adsorption of organic acids on magnetite nanoparticles, pH-dependent colloidal stability and salt tolerance, Colloids Surf. A 435 (2013) 91–96.

[20] H.P. Klug, L.E. Alexander, X-ray Diffraction Procedures for Polycrystalline and Amorphous Materials, 2nd ed., Wiley-Interscience, S.l., 1974.

[21] G. Muscas, G. Singh, W.R. Glomm, R. Mathieu, P.A. Kumar, G. Concas, E. Agostinelli, D. Peddis, Tuning the Size and Shape of Oxide Nanoparticles by Controlling Oxygen Content in the Reaction Environment: Morphological Analysis by Aspect Maps, Chem. Mater. 27 (6) (2015) 1982–1990.

[22] C.A. Schneider, W.S. Rasband, K.W. Eliceiri, NIH Image to ImageJ: 25 years of image analysis, Nat. Methods. 9 (7) (2012) 671–675.

[23] W.B. White, B.A. DeAngelis, Interpretation of the vibrational spectra of spinels, Spectrochim. Acta A 23 (4) (1967) 985–995.

[24] J.M. Byrne, V.S. Coker, S. Moise, P.L. Wincott, D.J. Vaughan, F. Tuna, E. Arenholz, G. van der Laan, R.A.D. Pattrick, J.R. Lloyd, N.D. Telling, Controlled cobalt doping in biogenic magnetite nanoparticles, J. Royal Soc. Interface 10 (83) (2013) 20130134.

[25] M. Walker, P.I. Mayo, K. O'Grady, S.W. Charles, R.W. Chantrell, The magnetic properties of single-domain particles with cubic anisotropy. I. Hysteresis loops, J. Phys. Condens. Matter 5 (17) (1993) 2779.

[26] B. Issa, I.M. Obaidat, B.A. Albiss, Y. Haik, Magnetic nanoparticles: Surface effects and properties related to biomedicine applications, Int. J. Mol. Sci. (11) (2013) 21266–21305.

[27] P.D. Thang, G. Rijnders, D.H. Blank, Spinel cobalt ferrite by complexometric synthesis, J. Magn. Magn. Mater. 295 (3) (2005) 251–256.

[28] J.B. Lambert, Introduction to organic spectroscopy, Macmillan; Collier Macmillan, New York, 1987.

[29] Z. Chen, L. Gao, Synthesis and magnetic properties of $CoFe_2O_4$ nanoparticles by using PEG as surfactant additive, Mater. Sci. Eng. B. 141 (1-2) (2007) 82–86.

[30] M. Vadivel, R.R. Babu, M. Arivanandhan, K. Ramamurthi, Y. Hayakawa, Role of SDS surfactant concentrations on the structural, morphological, dielectric and magnetic properties of $CoFe_2O_4$ nanoparticles, RSC Adv. 5 (34) (2015) 27060–27068.

Figure captions

Figure 1 Structural and microstructural characterisation of $Co_xFe_{3-x}O_4$; (a) XRPD patterns; (b) Gradual shift of the (311) XRPD peak position with various Co^{2+} content; (c) TEM micrographs; (d) Log-normal distribution functions from fitting the TEM particle size data and (e) magnification of the fingerprint range of the FT-IR spectra showing the metal-oxygen stretching

Figure 2 Magnetic characterisation; (a) Magnetisation vs. magnetic field curves at 300 K; (b) Temperature dependence of the ZFC/FC magnetisation of the $Co_xFe_{3-x}O_4$ (with x = 0.1, 0.2 and 1)

Figure 3 Structural and microstructural properties of $CoFe_2O_4$ samples prepared without or with different surfactants; (a) XRPD patterns; (b) FT-IR spectra with the assignments of the most relevant vibrational modes; (c) TEM micrographs and (d) Log-normal distribution functions from fitting the TEM particle size data

Tables

Table 1. Chemical composition and structural/microstructural properties of $Co_xFe_{3-x}O_4$ (PEG 300 in reaction mixture).

Sample (Targeted)	Chemical composition (ICP-OES)	$<D_{XRPD}>$ (nm)	a (Å)	$<D_{TEM}>$ (nm)	σ_{TEM} (%)	D_h (nm)	σ_h (%)
Fe_3O_4	Fe_3O_4	17.1(0)	8.374(9)	20.1	19	268	25.2
$Co_{0.1}Fe_{2.9}O_4$	$Co_{0.10}Fe_{2.90}O_4$	18.7(7)	8.360(5)	26.5	30	304	16.6
$Co_{0.2}Fe_{2.8}O_4$	$Co_{0.20}Fe_{2.80}O_4$	17.5(6)	8.366(7)	24.8	26	335	11.8
$CoFe_2O_4$	$Co_{0.98}Fe_{2.02}O_4$	6.6(8)	8.371(9)	8.2	26	205	36.5

Table 2. Magnetic properties of $Co_xFe_{3-x}O_4$ at 300 K: H_c, M_r, M_s, and M_r/M_s.

Sample	H_c (Oe)	M_r (emu g^{-1})	M_s (emu g^{-1})	M_r/M_s
Fe_3O_4	91±1	9.98±0.02	73.3±0.1	0.14±0.02
$Co_{0.1}Fe_{2.9}O_4$	526±5	26.44±0.02	76.2±0.1	0.35±0.02
$Co_{0.2}Fe_{2.8}O_4$	1070±10	31.86±0.02	77.8±0.3	0.41±0.07
$CoFe_2O_4$	189±2	7.10±0.02	71.7±0.1	0.10±0.02

Table 3. Chemical composition and structural/microstructural parameters of $CoFe_2O_4$ samples prepared with different surfactants (see text).

Sample	Chemical composition (ICP-OES)	$\langle D_{XRPD} \rangle$ (nm)	a (Å)	$\langle D_{TEM} \rangle$ (nm)	σ_{TEM} (%)
$CoFe_2O_4$	$Co_{0.983}Fe_{2.017}O_4$	7.9(5)	8.359(4)	12.2	25
$CoFe_2O_4$_PEG 300	$Co_{0.978}Fe_{2.022}O_4$	6.6(8)	8.371(9)	8.2	26
$CoFe_2O_4$_PEG 4000	$Co_{0.975}Fe_{2.025}O_4$	6.4(5)	8.381(1)	8.2	26
$CoFe_2O_4$_SDS	$Co_{0.981}Fe_{2.019}O_4$	5.8(8)	8.382(4)	8.4	34

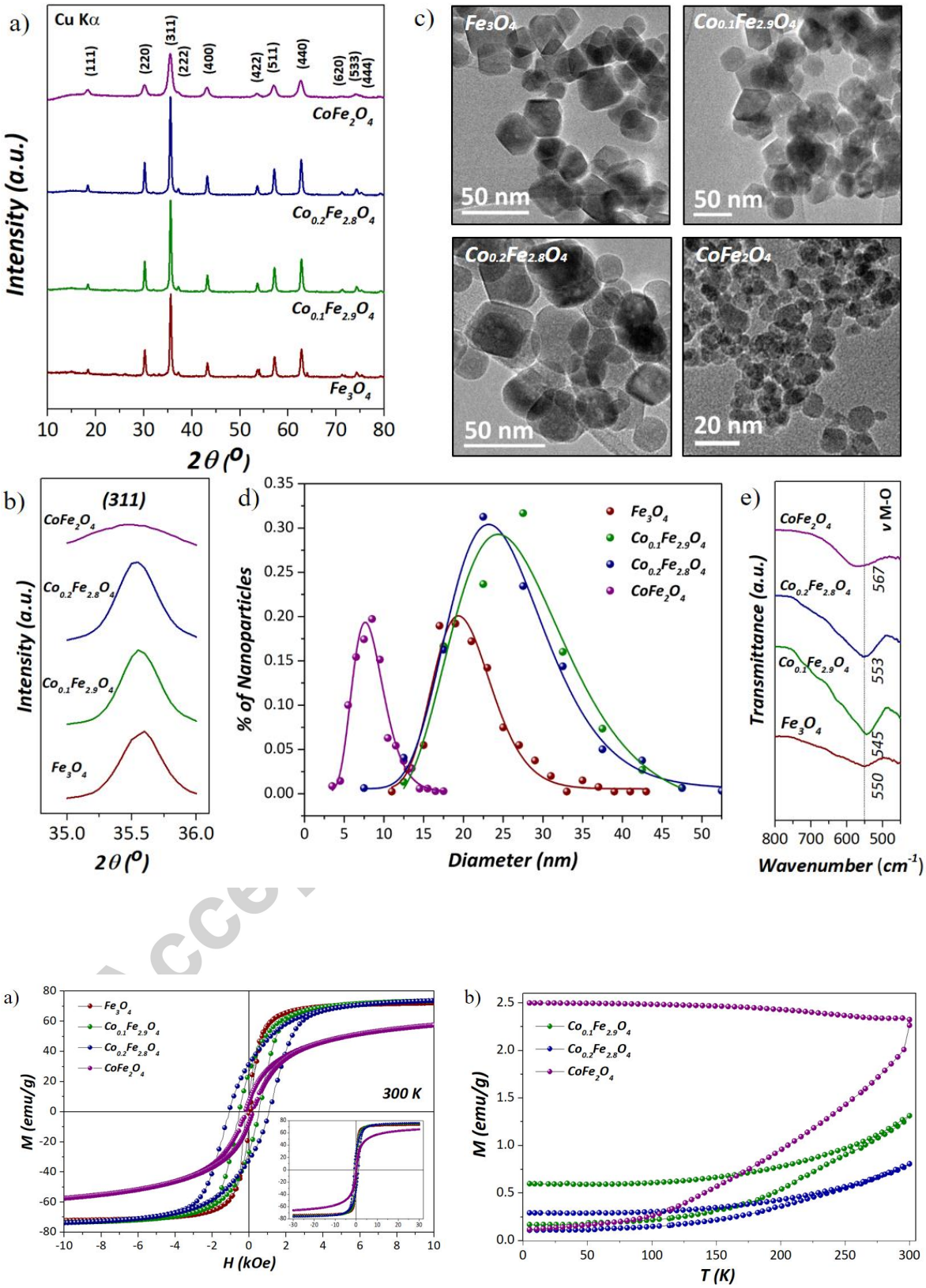
a)
Cu Kα
(111)
(220)
(311)
(222)
(400)
(422)
(511)
(440)
(620)
(533)
(444)
CoFe2O4
Co0.2Fe2.8O4
Co0.1Fe2.9O4
Fe3O4
Intensity (a.u.)
2θ (O)
c)
Fe3O4
Co0.1Fe2.9O4
Co0.2Fe2.8O4
CoFe2O4
50 nm
50 nm
50 nm
20 nm
b)
(311)
CoFe2O4
Co0.2Fe2.8O4
Co0.1Fe2.9O4
Fe3O4
Intensity (a.u.)
2θ (O)
d)
Fe3O4
Co0.1Fe2.9O4
Co0.2Fe2.8O4
CoFe2O4
% of Nanoparticles
Diameter (nm)
e)
CoFe2O4
Co0.2Fe2.8O4
Co0.1Fe2.9O4
Fe3O4
ν M-O
567
553
545
550
Transmittance (a.u.)
Wavenumber (cm-1)

a)
Fe3O4
Co0.1Fe2.9O4
Co0.2Fe2.8O4
CoFe2O4
300 K
M (emu/g)
H (kOe)
b)
Co0.1Fe2.9O4
Co0.2Fe2.8O4
CoFe2O4
M (emu/g)
T (K)

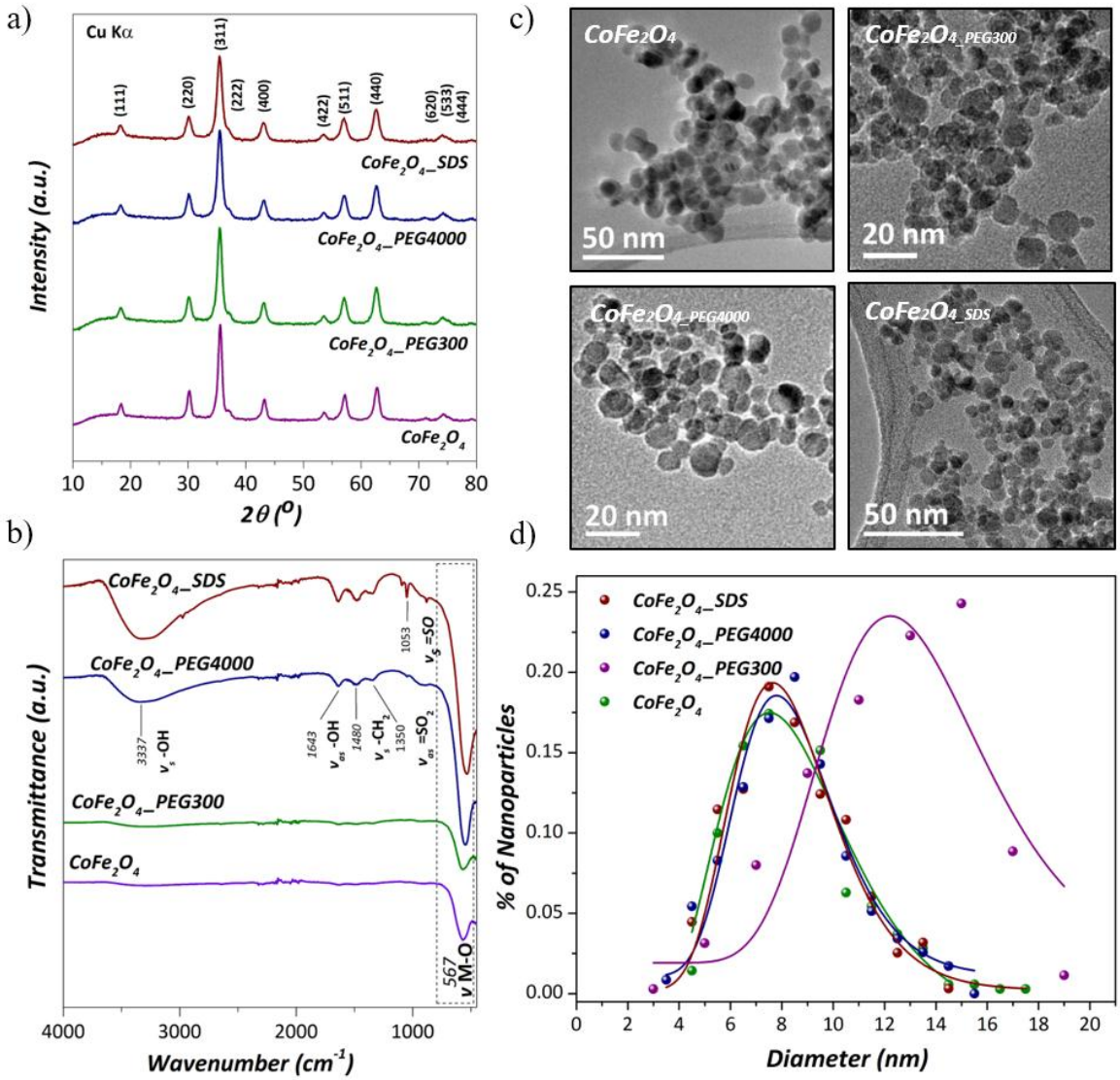
a)
Cu Kα
(111)
(220)
(311)
(222)
(400)
(422)
(511)
(440)
(620)
(533)
(444)
CoFe2O4_SDS
CoFe2O4_PEG4000
CoFe2O4_PEG300
CoFe2O4
Intensity (a.u.)
10 20 30 40 50 60 70 80
2θ (°)
b)
CoFe2O4_SDS
CoFe2O4_PEG4000
CoFe2O4_PEG300
CoFe2O4
3337 ν s -OH
1643 ν as -OH
1480 ν s -CH2
1350 ν as =SO2
1053 ν s =SO
567 ν M-O
Transmittance (a.u.)
4000 3000 2000 1000
Wavenumber (cm-1)
c)
CoFe2O4
50 nm
CoFe2O4_PEG300
20 nm
CoFe2O4_PEG4000
20 nm
CoFe2O4_SDS
50 nm
d)
CoFe2O4_SDS
CoFe2O4_PEG4000
CoFe2O4_PEG300
CoFe2O4
% of Nanoparticles
0.25 0.20 0.15 0.10 0.05 0.00
0 2 4 6 8 10 12 14 16 18 20
Diameter (nm)